Direct observation of anisotropic magnetic field response of the spin helix in FeGe thin films

N. Kanazawa, J. S. White, H. M. Rønnow, C. D. Dewhurst, Y. Fujishiro, A. Tsukazaki, Y. Kozuka, M. Kawasaki, M. Ichikawa, F. Kagawa, and Y. Tokura

Phys. Rev. B **94**, 184432 — Published 28 November 2016

DOI: 10.1103/PhysRevB.94.184432

Direct observation of the anisotropic magnetic field response of the spin helix in FeGe thin film

N. Kanazawa*,[1] J. S. White*,[2] H. M. Rønnow,[3] C. D. Dewhurst,[4] Y. Fujishiro,[1] A. Tsukazaki,[5] Y. Kozuka,[1] M. Kawasaki,[1,6] M. Ichikawa,[1] F. Kagawa,[6] and Y. Tokura[1,6]

[1]*Department of Applied Physics and Quantum Phase Electronics Center (QPEC), University of Tokyo, Tokyo 113-8656, Japan*

[2]*Laboratory for Neutron Scattering and Imaging (LNS), Paul Scherrer Institute (PSI), CH-5232 Villigen, Switzerland*

[3]*Laboratory for Quantum Magnetism (LQM), Institute of Physics, École Polytechnique Fédérale de Lausanne (EPFL), CH-1015 Lausanne, Switzerland*

[4]*Institut Laue-Langevin, 6 rue Jules Horowitz 38042 Grenoble, France*

[5]*Institute for Materials Research, Tohoku University, Sendai 980-8577, Japan*

[6]*RIKEN Center for Emergent Matter Science (CEMS), Wako, 351-0198, Japan*

(Dated: October 28, 2016)

Abstract

We report the observation by small-angle neutron scattering (SANS) of a magnetic helical structure confined in a thin film of the chiral lattice magnet FeGe. Two-fold magnetic Bragg spots appearing below the magnetic transition temperature indicate the formation of a spin helix with a single propagation vector $\boldsymbol{q}$ aligned perpendicular to the film plane. Due to magnetic anisotropy, the direction of $\boldsymbol{q}$ is unaffacted by an external magnetic field $\boldsymbol{H}$. Instead we observe anisotropic deformations of the spin helix with respect to the $\boldsymbol{H}$-direction. In the configuration with $\boldsymbol{H} \perp \boldsymbol{q}$, the helical pitch exhibits hysteretic elongation with $\boldsymbol{H}$, while the system tends to maintain an integer number of spiral turns within the film thickness by continuously pushing out one turn. For $\boldsymbol{H} \parallel \boldsymbol{q}$, the helix is smoothly distorted to a conical structure with minimal change in the magnetic period. The direct measurement of $\boldsymbol{q}$ by SANS establishes a correspondence between helix deformation and macroscopic features observed in magnetization and magnetoresistivity.

PACS numbers: 75.25.-j, 75.70.-i, 72.15.Gd

* These two authors equally contributed to this work.

INTRODUCTION

Spiral spin orders produce a variety of functional responses via interaction with electronic states. Spontaneous electric polarization can arise in association with broken inversion symmetry due to the formation of spiral spin orders [1]. The coexistence of ferroelectric and magnetic orders, so-called multiferroicity, allows mutual control of magnetism and electricity, i.e., electrically induced magnetization and magnetically induced polarization. Another striking example is the formation of topological spin textures such as skyrmions [2–4]. Helical spin structures are an essential ingredient for the formation of skyrmion lattices, which can be viewed as mode-coupling between three helical spin structures whose modulation vectors $\boldsymbol{q}$ are rotated by 120° [3, 5–7]. Emergent electromagnetic fields mediating the coupling between conduction electrons and skyrmions give rise to characteristic transport phenomena [8], such as the topological Hall effect [9–11] and the efficient electrical drive of skyrmions [12, 13]. The above functional properties have the potential to serve as key ingredients for power efficient magnetic storage devices [14–16].

A deformed helical spin structure called helicoidal structure [17–19] also induces characteristic transport properties [20–23]. In the chiral magnet $CrNb_3S_6$, the Dzyaloshinskii-Moriya (DM) interaction stabilizes a helical spin structure [24, 25]. Due to the strong planar magnetic anisotropy, $\boldsymbol{q}$ and spin spiral plane are aligned parallel and perpendicular to the chiral axis, respectively. A magnetic field applied perpendicular to the helical modulation direction ($\boldsymbol{H} \perp \boldsymbol{q}$) expands the portion of magnetic moments tilted toward $\boldsymbol{H}$, which consequently elongates the helicoidal period without inclination of propagation direction [26]. This deformed state can be regarded as a periodic array of 2π-spin-rotation kinks intervening between *ferromagnetic* domains; and therefore it is also called chiral magnetic soliton lattice (CSL). In the CSL state, the magnetoresistivity (MR) changes in proportion to the number of the magnetic kinks which can be tuned with variation of H [27]. In particular, discrete changes in the number of solitons become discernible as a stepwise H-dependence of MR when the sample size is approximately as small as several magnetic periods [28]. Such discrete electromagnetic responses inspire ideas for binary or multivalued information bits in storage devices.

On this basis, for practical use there is a demand for the realization of epitaxial thin films exhibiting the helicoidal state. Magnetization (M), MR, and polarized neutron reflectometry

(PNR) measurements have indicated that helical spin structures confined in thin films of B20 chiral magnets (MnSi and FeGe) undergo helicoidal deformation and also show discrete dependency of helicoidal period with variation of H [29, 30]. Furthermore, such deformation process can be controlled by modifying the boundary condition via exchange coupling with an adjacent ferromagnetic layer [30].

Here we report the direct observation by small-angle neutron scattering (SANS) of the propagation vector $\boldsymbol{q}$ of the helical spin state in FeGe thin films as a function of magnetic field. The evolution of $\boldsymbol{q}$ indicates the helical structure propagating along the film normal at zero field to exhibit anisotropic deformation behaviors with respect to the direction of magnetic field: namely, the formation of the helicoidal state under $\boldsymbol{H} \perp \boldsymbol{q}$ and the conical state under $\boldsymbol{H} \parallel \boldsymbol{q}$. Our detailed SANS measurements show directly that q of helicoidal structure changes continuously with H, contrary to a previous study on MnSi thin films where discrete changes in q are reported [29]. Despite the continuous change in helicoidal period, M and MR change more rapidly with small variations of H, exhibiting stepwise profiles associated with the number of helicoidal turns.

EXPERIMENTS

FeGe thin films were grown on highly resistive Si(111) substrates by means of molecular beam epitaxy [31]. We co-evaporated Fe and Ge onto a Si(111)-(7×7) surface heated at 325 °C. A θ-2θ x-ray diffraction scan verifies the epitaxial growth of B20-type FeGe with minimal impurity below the detection limit [Fig. 1(a)]. From the slightly broadened profile of the FeGe (132) peak in the reciprocal space mapping [Fig. 1(b)], we can estimate the strain in the FeGe film. Owing to the expected good lattice matching -0.05 %, the FeGe lattice is nearly consistent with that of bulk ($a_{\mathrm{bulk}} = 4.700$ Å) [32], but there can be seen slight tensile (0.33 %) and compressive (0.27 %) strain along out-of-plane and in-plane directions, respectively, presumably because of slight off-stoichiometry. Cross-sectional images of the FeGe thin film by transmission electron microscopy (TEM) [Fig. 1(c)] and energy dispersive x-ray spectroscopy (see Fig. 5 in Appendix A) identify slight diffusion of Fe into the Si substrate. The thickness of the FeGe film is determined as 206 nm from the TEM image [Fig. 1(c)].

To study the magnetic order directly in the FeGe thin films, we used the small-angle

neutron scattering (SANS) technique. Experiments were carried out using the D33 beamline at Institut Laue-Langevin (ILL), Grenoble, France, and the SANS-II instrument at the Swiss Spallation Neutron Source (SINQ), Paul Scherrer Institut (PSI), Switzerland. Neutron wavelengths of 6 Å and 20 Å were used at D33 and SANS-II respectively, and selected with an approximate 10 % FWHM spread. At D33 (SANS-II) the neutron beam was collimated over 12.8 m (6 m) before the sample. The scattered neutrons were detected using a position-sensitive two-dimensional multidetector placed behind the sample. The sample-to-detector distance equaled the incoming beam collimation length.

In order to accumulate sufficient neutron scattering signal, for the SANS experiment a sample was prepared by coaligning a stack of 32 FeGe films each 15×15 mm^2 size (substrate thickness is $\sim$ 0.28 mm), as schematically illustrated in Fig. 1(d). The total illuminated volume of FeGe was thus $\sim 1.5 \times 10^{-3}$ cm^3, which corresponds to a mass of FeGe of $\sim$ 12 mg. The film stack was installed into a horizontal field cryomagnet with the film [111] and [$\bar{1}$10] directions respectively perpendicular and parallel to the incoming neutron beam. SANS measurements were done by rotating the cryomagnet and sample ensemble together over a range of rotation (rocking) angles that moved the diffraction spots through the Bragg condition at the detector. Measurements in the magnetically-ordered state were carried out at various magnetic fields below the critical field and temperatures below $T_{\rm N}$. Further measurements recorded in the paramagnetic state above $T_{\rm N}$, or the field-polarized ferromagnetic (FM) state, were used as a background and subtracted from the low magnetic field, low temperature data in order to leave only the signal due to the magnetic order. The direction of the magnetic field could be rotated, and applied along the in-plane, or out-of-plane direction, i.e., parallel to the [$\bar{1}$10] or [111] direction, of the FeGe thin film respectively. We label these $\boldsymbol{H}_{\rm in}$ and $\boldsymbol{H}_{\rm out}$ [see Fig. 1(d)].

The origin of rocking angle is defined as when the incoming neutron beam is exactly parallel to the [$\bar{1}$10] direction of FeGe. Here we point out that the films contain two types of crystalline domains, which are related by 180°-rotation around the FeGe[111] direction (the film normal). The existence of the rotational domains does not affect following discussions because the spin helix, which modulates along the film normal, will not show a different response between $\boldsymbol{H} \parallel$ FeGe[$\bar{1}$10] and $\boldsymbol{H} \parallel$ FeGe[1$\bar{1}$0].

Magnetization and MR measurements were performed in the same magnetic-field configurations as SANS. A conventional four-terminal geometry was employed for MR measure-

ments.

RESULTS AND DISCUSSIONS

Figure 2(a) shows a SANS pattern taken at $T = 3$ K and $H = 0$ T, typical of those obtained below the magnetic transition temperature $T_{\rm N} = 280$ K. We observe a pair of magnetic Bragg peaks with a propagation vector aligned along the film normal of $|\boldsymbol{q}| = 8.77 \times 10^{-3}$ Å^{-1}; the propagation direction is pinned by magnetocrystalline anisotropy as well as by additional anisotropic effects due to the strain and shape of the thin film. This scattering pattern indicates the formation of a periodically-modulating magnetic structure at zero field, which should be a helical structure as is the case with B20-type bulk FeGe [33]. As presented in Fig. 2(b), the rocking profile of the magnetic Bragg peak is well fitted by a single Lorentzian function, demonstrating that the FeGe film hosts a state defined by a single helix. Temperature dependences of the scattering intensity and modulation vector are shown in Fig. 2(c) and Fig. 2(d), respectively. The scattering intensity scales accurately with the square of the saturated magnetization $M^2(T,\ H_{\rm in} = 0.2$ T) [also see Figs. 3(c) and 3(d)]. This verifies that the scattering is attributable to a magnetic origin. The magnitude of $\boldsymbol{q}$ is weakly temperature dependent, ranging from $q = 8.77 \times 10^{-3}$ Å^{-1} (magnetic modulation period $\lambda = 71.6$ nm) at 3 K to $q = 8.53 \times 10^{-3}$ Å ($\lambda = 73.7$ nm) at 270 K. The magnetic modulation period is almost identical to that of bulk FeGe ($\lambda_{\rm bulk} = 68.3$-$70.0$ nm) [33], in contrast to the case of MnSi films, where significant shrinkage of λ is induced due to additional magnetic anisotropy associated with the strain from the Si substrate [35, 36]. Modification of magnetic anisotropy in the FeGe thin film instead shows up as stronger pinning of helical modulation direction. In bulk FeGe, the $\boldsymbol{q}$-direction flops between $\langle 100 \rangle$ and $\langle 111 \rangle$ as the temperature varies at zero magnetic field [33]. In the thin film, the $\boldsymbol{q}$-direction remains aligned along the film normal, i.e., [111], over the entire temperature region below $T_{\rm N}$ and even under magnetic fields as described below.

Next we describe how the helical structure in FeGe thin film undergoes deformations with respect to the magnetic field direction. We recorded SANS patterns in both $\boldsymbol{H}_{\rm in}$ and $\boldsymbol{H}_{\rm out}$ configurations, and by decreasing the magnetic field from large positive fields above the critical fields, i.e., 0.25 T for $\boldsymbol{H}_{\rm in}$ and 1.0 T for $\boldsymbol{H}_{\rm out}$. For the $\boldsymbol{H}_{\rm in}$ and $\boldsymbol{H}_{\rm out}$ configurations, the critical fields separating the helicoidal and field-polarized ferromagnetic (FM) state are

different mainly due to demagnetization effect [also see M-H curves in Figs. 3(c) and 3(d)]. On application of an in-plane magnetic field $\boldsymbol{H}_{\rm in}$, the magnitude of $\boldsymbol{q}$ changes without inclination of its direction as presented in the example SANS patterns of Figs. 3(g)-3(j). On the other hand, under an out-of-plane field $\boldsymbol{H}_{\rm out}$, $\boldsymbol{q}$ remains almost identical to that at $H = 0$. Figures 3(a) and 3(b) show detailed H-dependences of λ under $\boldsymbol{H}_{\rm in}$ and $\boldsymbol{H}_{\rm out}$, respectively. In contrast to the constant λ ($\lambda_0 = 72$ nm) under $\boldsymbol{H}_{\rm out}$, λ shows an asymmetric variation about zero field with decreasing $\boldsymbol{H}_{\rm in}$, where we denote characteristic fields as H_i (i = 1-6) [Fig. 3(a)]: (i) For $H_1 > H > H_2$, λ is approximately $1.5\lambda_0 = 108$ nm, i.e., two turns of helix are accommodated along the film thickness. (ii) For $H_2 > H > H_3$, λ gradually changes toward its zero-field value of λ_0 with decreasing H. (iii) For $H_3 > H > H_4$, λ ($\approx \lambda_0$) depends only weakly on H, where the helical structure modulates by three periods. (iv) For $H_4 > H > H_5$, λ continuously changes back to $1.5\lambda_0$ as in the high positive fields, (v) For $H_5 > H > H_6$, λ stays at $1.5\lambda_0$, where the two-turns spiral state is maintained until the transition to the forced ferromagnetic state occurs.

Full determination of the internal spin structure of the spin helix requires further intensity measurements by SANS. Nevertheless we can assume that the helical structure is deformed into a conical structure by $\boldsymbol{H}_{\rm out}$ and a helicoidal CSL structure by $\boldsymbol{H}_{\rm in}$ on the basis of the above H-dependences of λ. $\boldsymbol{H}_{\rm out} \parallel \boldsymbol{q}$ tilts the magnetic moments toward its direction, resulting in deformation of the spin spiral plane to an umbrella shape without change in the magnetic period. On the other hand, $\boldsymbol{H}_{\rm in} \perp \boldsymbol{q}$ increases the population of magnetic moments tilted toward the field direction, leading to the realization of a helicoidal structure with expanded magnetic period as is the case of $CrNb_3S_6$ [26].

The anisotropic magnetic field responses of the spin helix are further manifested by sharp differences between physical properties under $\boldsymbol{H}_{\rm in}$ and $\boldsymbol{H}_{\rm out}$. Figures 3(c)-3(f) show the H-dependences of M and MR in the respective configurations. An obvious difference is identified in their hysteresis behavior. As expected from the asymmetric profile of λ under $\boldsymbol{H}_{\rm in}$, M and MR respectively display clear hysteretic behaviors that appear as the difference between the decreasing-H process (blue/red curves) and the increasing-H process (gray curves) in Figs. 3(c) and 3(e). In contrast, no distinct hysteresis behavior is observed in the $\boldsymbol{H}_{\rm out}$-configuration except for a faint hysteresis loop of M-H curve at low fields, which may suggest a tiny hysteretic response of the spiral spin plane.

Another distinctive difference is discerned in the H-dependence of M and MR. Under

$\boldsymbol{H}_{\rm in}$, both of M and MR show abrupt changes with steep steps at H_2 and H_5, and with tendency to plateau for H-regions of $H_2 > H > H_3$ and $H_4 > H > H_5$ [Figs. 3(c) and 3(e)], where λ varies continuously. Under $\boldsymbol{H}_{\rm out}$, the smooth H-dependence of M and MR indicates a continuous evolution of the cone angle. Here the magnetic field closes the umbrella of the spin spiral plane, resulting in a H-linear profile of M and a conventional negative MR proportional to M^2 below the critical field $H_{\rm c}$.

We confirmed that the H-dependent profiles of λ, M and MR are maintained over a wide temperature region below 250 K (see Fig. 6 in Appendix B for all the data sets at various temperatures), from which we can establish a magnetic phase diagram for the FeGe thin film. For the $\boldsymbol{H}_{\rm out}$ configuration, a single conical magnetic phase comprises the low-field region [Fig. 4(b)]. For the $\boldsymbol{H}_{\rm in}$ configuration, the plateaus in the λ-$\boldsymbol{H}_{\rm in}$ curves [Figs. 3(a) and 6] indicate that helicoidal states with three and two turns show local energy minima at low- and high-magnitude magnetic fields, respectively; i.e., helicoidal structures with a pitch commensurate with film thickness are energetically favored. These two commensurate phases are separated by an incommensurate phase, where λ is continuously tuned by $\boldsymbol{H}_{\rm in}$. The commensurate-incommensurate transitions are of the first-order as evidenced by the hysteresis behaviors of M and MR [Figs. 3(c) and 3(e)].

We note that the behavior of λ we observe for FeGe thin films with variation of $\boldsymbol{H}_{\rm in}$ appears to require an explanation that is different from the following intuitive scenario proposed to explain the discrete change in helicoidal period with H variation in MnSi thin film [29]: To exploit an free-energy gain from Zeeman energy, a helicoidal state with *half-integer* turns is likely to be realized, where the number of regions with magnetization tilted parallel to $\boldsymbol{H}$ exceeds by one that of antiparallel magnetization. According to this model, the helicoidal state *discontinuously* transforms between different half-integer-turn states with variation of H; e.g., in the case of MnSi thin film, the helicoidal structure transforms between states with 1.5 and 0.5 turns in a first-order manner, and without an intermediate incommensurate phase [29].

Contrary to the expected analogy to the MnSi films, helicoidal states with *integer* turns seems to be energetically favored in our FeGe thin films and the transformation between these integer-turn states is realized through an incommensurate state, whose helicoidal period is observed to *continuously* change with variation of $\boldsymbol{H}_{\rm in}$. In accord with remarkable differences observed in magnetic properties between MnSi and FeGe, e.g., saturated moment, helical

period, and so on [37], our measurements show that the magnetic boundary conditions that control the helicoidal order in thin films are also different [38, 39]. We thus propose that there may exist a periodic boundary condition, which can show up in a finite size system, so as to stabilize helicoidal states with integer periods in FeGe thin films. The origin of such a boundary condition can arise from spins at the film boundaries, which do not have neighboring spins to interact with, and so will tend to be aligned along magnetic field to profit from Zeeman energy [40].

CONCLUSIONS

Our SANS study on the FeGe thin film reveals the developments of the spin helix under in-plane ($\boldsymbol{H}_{\rm in}$) and out-of-plane magnetic fields ($\boldsymbol{H}_{\rm out}$). The helical structure at zero field is deformed to be a helicoidal (CSL) structure by $\boldsymbol{H}_{\rm in}$ or a conical structure by $\boldsymbol{H}_{\rm out}$, without inclination of the modulation direction ($\boldsymbol{q} \parallel$ film normal) in both cases. With variations of H, the conical period almost remain constant, whereas the helicoidal structure transforms between different states with three and two turns along the film thickness by continuously changing its period λ. The characteristic deformations manifest themselves in physical properties as anisotropic M and MR profiles: the smooth H-dependences in conical state and the stepwise rapid changes in H-regions where λ continuously varies. This correspondence between the number of helicoidal turns and the magnetic properties could possibly be utilized as binary or multivalued information bit for higher density recording. More multistep transformation of the helicoidal state is, however, required for the implementation of a practical application.

There are still future challenges to elucidate the internal spin arrangement, such as observation of higher harmonic order scattering by SANS and real-space imaging by transmission electron microscopy. The physical reason why an integer number of magnetic spiral turns is realized in the FeGe thin film also remains to be elucidated, and we have speculated about the importance of boundary conditions for the spin helix. To identify which physical parameters play important roles in this, simulations for a three-dimensional lattice spin model would be most important, as well as experimental observations, e.g. by various diffraction methods, of the spin helix unwinding process in chiral magnet thin films with varying thickness.

ACKNOWLEDGMENTS

This work is based on experiments performed at Institut Laue-Langevin (ILL), Grenoble, France and Paul Scherrer Institut (PSI), Villigen, Switzerland. The authors thank Y. Endoh, X. Z. Yu and T. Yokouchi for enlightening discussions. This work was partially supported by JSPS KAKENHI (Grant Nos. 24224009, 24226002, and 15H05456) and Swiss National Science Foundation.

APPENDIX A: ELEMENTAL ANALYSIS

We show in Fig. 5 annular dark field scanning transmission electron microscope (ADF-STEM) image and energy dispersive X-ray spectrometry (EDX) mappings for Si, Fe, and Ge elements of the FeGe thin film.

APPENDIX B: MAGNETIC-FIELD DEPENDENCES OF MAGNETIC PROPERTIES AT VARIOUS TEMPERATURES

We show in Fig. 6 detailed magnetic-field dependences of the magnetic modulation period λ, magnetization M, and magnetoresistivity under in-plane ($\boldsymbol{H}_{\rm in}$) and out-of-plane ($\boldsymbol{H}_{\rm out}$) magnetic fields at various temperatures of $T = 100$, 200, and 250 K.

[1] Y. Tokura and S. Seki, Adv. Mater. **22**, 1554-1565 (2010).

[2] A. N. Bogdanov and D. A. Yablonskii, Sov. Phys. JETP **68**, 101 (1989).

[3] S. Mühlbauer, B. Binz, F. Jonietz, C. Pfleiderer, A. Rosch, A. Neubauer, R. Georgii, and P. Böni, Science **323**, 915 (2009).

[4] X. Z. Yu, Y. Onose, N. Kanazawa, J. H. Park, J. H. Han, Y. Matsui, N. Nagaosa, and Y. Tokura, Nature **465**, 901 (2010).

[5] T. Adams, S. Mühlbauer, C. Pfleiderer, F. Jonietz, A. Bauer, A. Neubauer, R. Georgii, P. Böni, U. Keiderling, K. Everschor, M. Garst, and A. Rosch, Phys. Rev. Lett. **107**, 217206 (2011).

[6] D. McGrouther, R. J. Lamb, M. Krajnak, S. McFadzean, S. McVitie, R. L. Stamps, A. O. Leonov, A. N. Bogdanov, and Y. Togawa, New J. Phys. **18**, 095004 (2016).

[7] K. Shibata, A. Kovács, N. Kanazawa, R. E. Dunin-Borkowski, and Y. Tokura, arXiv:1606.05723.

[8] N. Nagaosa and Y. Tokura, Nature Nanotechnol. **8**, 899 (2013).

[9] A. Neubauer, C. Pfleiderer, B. Binz, A. Rosch, R. Ritz, P. G. Niklowitz, and P. Böni, Phys. Rev. Lett. **102**, 186602 (2009).

[10] M. Lee, W. Kang, Y. Onose, Y. Tokura, and N. P. Ong, Phys. Rev. Lett. **102**, 186601 (2009).

[11] N. Kanazawa, Y. Onose, T. Arima, D. Okuyama, K. Ohoyama, S. Wakimoto, K. Kakurai, S. Ishiwata, and Y. Tokura, Phys. Rev. Lett. **106**, 156603 (2011).

[12] F. Jonietz, S. Mühlbauer, C. Pfleiderer, A. Neubauer, W. Münzer, A. Bauer, T. Adams, R. Georgii, P. Böni, R. A. Duine, K. Everschor, M. Garst, and A. Rosch, Science **330**, 1648 (2010).

[13] X. Z. Yu, N. Kanazawa, W. Z. Zhang, T. Nagai, T. Hara, K. Kimoto, Y. Matsui, Y. Onose, and Y. Tokura, Nature Commun. **3**, 988 (2012).

[14] A. Fert, V. Cros, and J. Sampaio, Nature Nanotechnol. **8**, 152 (2013).

[15] W. Koshibae, Y. Kaneko, J. Iwasaki, M. Kawasaki, Y. Tokura, and N. Nagaosa, Jpn. J. Appl. Phys. **54**, 053001 (2015).

[16] R. Wiesendanger, Nature Reviews Materials **1**, 16044 (2016).

[17] I. E. Dzyaloshinskii, Sov. Phys. JETP **19**, 960 (1964); I. E. Dzyaloshinskii, Sov. Phys. JETP **20**, 665 (1965).

[18] Y. A. Izyumov, Sov. Phys. Usp. **27**, 845 (1984).

[19] J.-i. Kishine, K. Inoue, and Y. Yoshida, Prog. Theor. Phys. Suppl. **159**, 82 (2005).

[20] I. G. Bostrem, J.-i. Kishine, and A. S. Ovchinnikov, Phys. Rev. B **78**, 064425 (2008).

[21] A. B. Borisov, J.-i. Kishine, I. G. Bostrem, and A. S. Ovchinnikov, Phys. Rev. B **79**, 134436 (2009).

[22] J.-i. Kishine, A. S. Ovchinnikov, and I. V. Proskurin, Phys. Rev. B **82**, 064407 (2010).

[23] J.-i. Kishine, I. V. Proskurin, and A. S. Ovchinnikov, Phys. Rev. Lett. **107**, 017205 (2011).

[24] T. Moriya and T. Miyadai, Solid State Commun. **42**, 209 (1982).

[25] T. Miyadai, K. Kikuchi, H. Kondo, S. Sakka, M. Arai, and Y. Ishikawa, J. Phys. Soc. Jpn. **52**, 1394 (1983).

[26] Y. Togawa, T. Koyama, K. Takayanagi, S. Mori, Y. Kousaka, J. Akimitsu, S. Nishihara, K. Inoue, A. S. Ovchinnikov, and J.-i. Kishine, Phys. Rev. Lett. **108**, 107202 (2012).

[27] Y. Togawa, Y. Kousaka, S. Nishihara, K. Inoue, J. Akimitsu, A. S. Ovchinnikov, and J.-i. Kishine, Phys. Rev. Lett. **111**, 197204 (2013).

[28] Y. Togawa, T. Koyama, Y. Nishimori, Y. Matsumoto, S. McVitie, D. McGrouther, R. L. Stamps, Y. Kousaka, J. Akimitsu, S. Nishihara, K. Inoue, I. G. Bostrem, Vl. E. Sinitsyn, A. S. Ovchinnikov, and J.-i. Kishine, Phys. Rev. B **92**, 220412(R) (2015).

[29] M. N. Wilson, E. A. Karhu, D. P. Lake, A. S. Quigley, S. Meynell, A. N. Bogdanov, H. Fritzsche, U. K. Rößler, and T. L. Monchesky, Phys. Rev. B **88**, 214420 (2013).

[30] N. A. Porter, C. S. Spencer, R. C. Temple, C. J. Kinane, T. R. Charlton, S. Langridge, and C. H. Marrows, Phys. Rev. B **92**, 144402 (2015).

[31] N. Kanazawa, M. Kubota, A. Tsukazaki, Y. Kozuka, K. S. Takahashi, M. Kawasaki, M. Ichikawa, F. Kagawa, and Y. Tokura, Phys. Rev. B **91**, 041122(R) (2015).

[32] M. Richardson, Acta Chem. Scand. **21**, 753 (1967).

[33] B. Lebech, J. Bernhard, and T. Freltoft, J. Phys.: Condens. Matter **1**, 6105 (1989).

[34] Broad rocking profiles of the magnetic Bragg spots [Fig. 2(b)] allow us to obtain almost symmetric scattering pattern [Fig. 2(a)] at the offset rocking angle $\omega = -4^\circ$.

[35] E. A. Karhu, S. Kahwaji, M. D. Robertson, H. Fritzsche, B. J. Kirby, C. F. Majkrzak, and T. L. Monchesky, Phys. Rev. B **84**, 060404(R) (2011).

[36] Y. Li, N. Kanazawa, X. Z. Yu, A. Tsukazaki, M. Kawasaki, M. Ichikawa, X. F. Jin, F. Kagawa, and Y. Tokura, Phys. Rev. Lett. **110**, 117202 (2013).

[37] Saturated magnetic moments of MnSi and FeGe are 0.4 μ_B/f.u. and 1.0 μ_B/f.u., respectively. Helical periods of MnSi and FeGe are 18 nm and 70 nm, respectively. [A. Bauer *et al.*, Phys. Rev. B **82**, 064404 (2010); L. Lundgren, K. Å. Blom, and O. Beckman, Phys. Lett. **28A**, 175 (1968); Y. Ishikawa *et al.*, Solid State Commun. **19**, 525 (1976).]

[38] J.-i. Kishine, I. G. Bostrem, A. S. Ovchinnikov, and Vl. E. Sinitsyn, Phys. Rev. B **89**, 014419 (2014).

[39] S. A. Meynell, M. N. Wilson, H. Fritzsche, A. N. Bogdanov, and T. L. Monchesky, Phys. Rev. B **90**, 014406 (2014).

[40] S. Buhrandt and L. Fritz, Phys. Rev. B **88**, 195137 (2013).

Figures

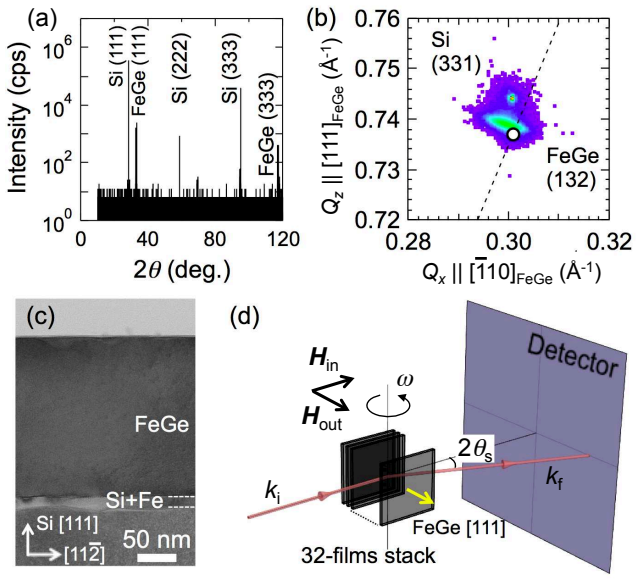

FIG. 1: (color online). (a) θ-2θ X-ray diffraction pattern of the FeGe thin film. (b) Reciprocal-space map around the Si (331) peak. The peak position estimated from the lattice parameter of bulk FeGe is indicated by an open circle. (c) Cross-sectional transmission electron microscopy image. (d) Experimental setup for the SANS experiment. The stack of 32 thin films of 15 mm $\times$ 15 mm size are aligned with their surfaces along the incident neutron beam when the rocking angle is zero. Magnetic fields were applied both parallel ($\boldsymbol{H}_{\rm in}$) and perpendicular ($\boldsymbol{H}_{\rm out}$) to the film surfaces.

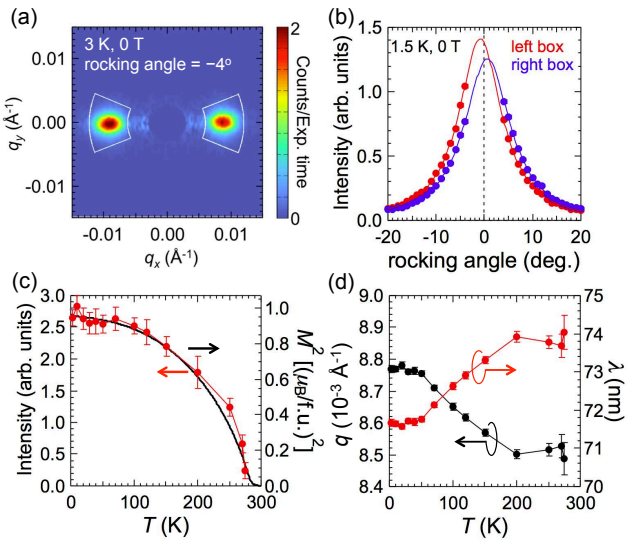

FIG. 2: (color online). (a) Typical SANS pattern at zero magnetic field. Due to the strong reflected neutron intensity from the periodic array of Si substrates, the magnetic Bragg scattering is discerned above a small offset rocking angle ($\approx \pm 4°$) [34]. (b) Rocking scan of magnetic Bragg peaks. Intensities in the left and right boxes in panel (a) are indicated by red and blue markers, respectively. Both rocking profiles are well fitted by single Lorentzians. (c) Temperature dependence of magnetic scattering intensity, which corresponds to magnetization profile ($\propto M^2$). (d) Weakly temperature-dependent magnetic propagation vector q. Scattering pattern at 290 K and 0T at a respective rocking angle was used as a background subtracted from the measured patterns below T_N.

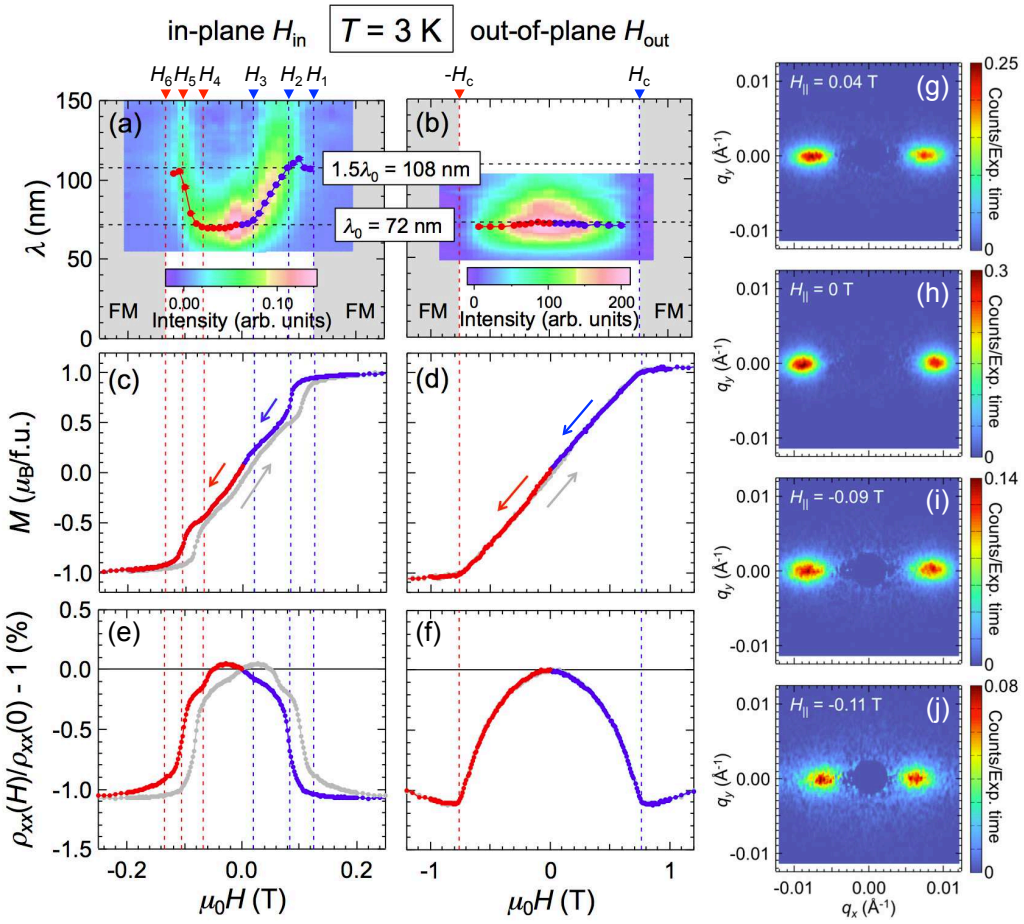
in-plane H_{in}
T = 3 K
out-of-plane H_{out}
H_6 H_5 H_4 H_3 H_2 H_1
$-H_c$
H_c
(a)
(b)
$1.5\lambda_0$ = 108 nm
λ_0 = 72 nm
λ (nm)
FM
Intensity (arb. units)
(c)
(d)
M (μ_B/f.u.)
(e)
(f)
$\rho_{xx}(H)/\rho_{xx}(0)$ - 1 (%)
$\mu_0 H$ (T)
$H_{||}$ = 0.04 T
(g)
$H_{||}$ = 0 T
(h)
$H_{||}$ = -0.09 T
(i)
$H_{||}$ = -0.11 T
(j)
q_y (Å^{-1})
q_x (Å^{-1})
Counts/Exp. time

FIG. 3: (color online). Magnetic-field dependences of the magnetic modulation period λ [(a) and (b)], magnetization M [(c) and (d)], and magnetoresistivity [(e) and (f)] under in-plane and out-of-plane fields at 2 K. In the background of panels (a) and (b), we show scattering intensity distribution maps as a function of λ at various magnetic fields. The color maps are produced from the radial dependence of scattering intensity in the reciprocal space (q_x, q_y) by conversion via the relation $\lambda = 2\pi/q$. At characteristic magnetic fields during decreasing-field processes, which are respectively labelled as H_i (i = 0-6) for $\boldsymbol{H}_{\rm in}$ configurations, following features are identified: At H_1, a pair of magnetic Bragg spots become discerned and M and MR start to exhibit gradual decrease and increase, respectively. At H_2, the Bragg spots begin to change their positions and M and MR show abrupt variations. At H_3, change in positions of the Bragg spots ceases and both H-dependence of M and MR indicates small kinks. At H_4, positions of the Bragg spots start to change again and stepwise variations of M and MR profiles set off. At H_5, change in positions of the Bragg spots ceases and M and MR show abrupt variations. At H_6, the Bragg spots disappear and variations of M and MR with variation of H become reduced. (g)-(j) Example SANS patterns for the development of helicoidal state with decreasing $\boldsymbol{H}_{\rm in}$: (g) $H_2 > 0.04$ T $> H_3$; (h) $H_3 > 0$ T $> H_4$; (i) $H_4 > -0.09$ T $> H_5$; (j) $H_5 > -0.11$ T $> H_6$. Scattering patterns at $T = 2$ K and $\mu_0 H_{\rm in} = 0.25$ T and at $T = 2$ K and $\mu_0 H_{\rm out} = 1.0$ T were used as a background subtracted from the measured patterns under respective field directions.

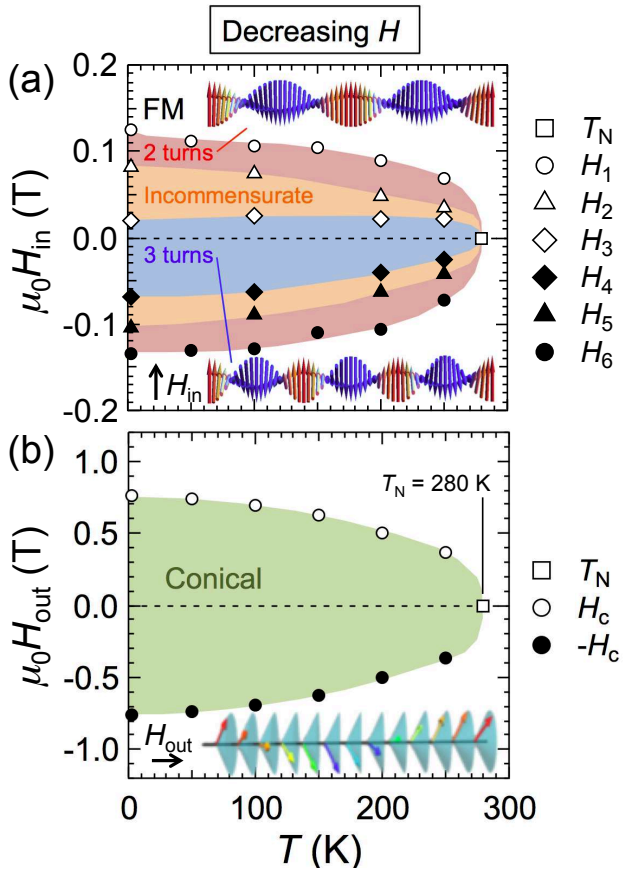

FIG. 4: (color online). Magnetic phase diagrams under decreasing (a) $\boldsymbol{H}_{\rm in}$ and (b) $\boldsymbol{H}_{\rm out}$ from large magnetic fields (e.g., $\boldsymbol{H}_{\rm in}$ = 0.25 T and $\boldsymbol{H}_{\rm out}$ = 1.0 T). Schematic illustrations of helicoidal and conical states are inset in panels (a) and (b), respectively.

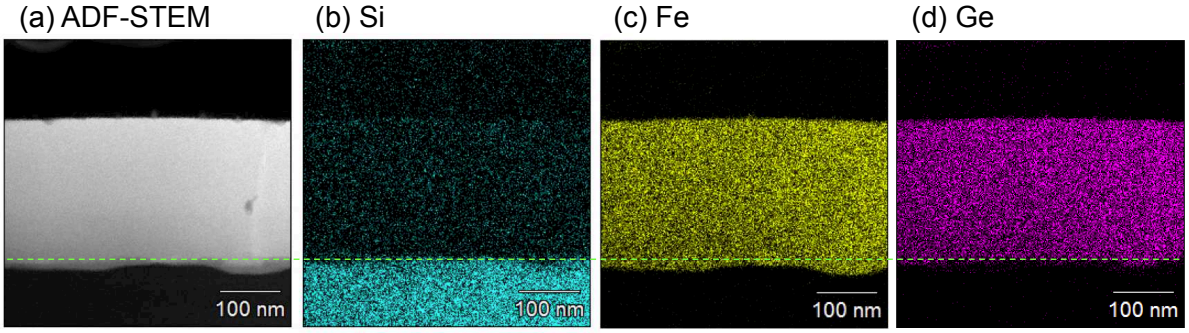

FIG. 5: (a) ADF-STEM image and (b)-(d) EDX mappings for Si, Fe, and Ge elements.

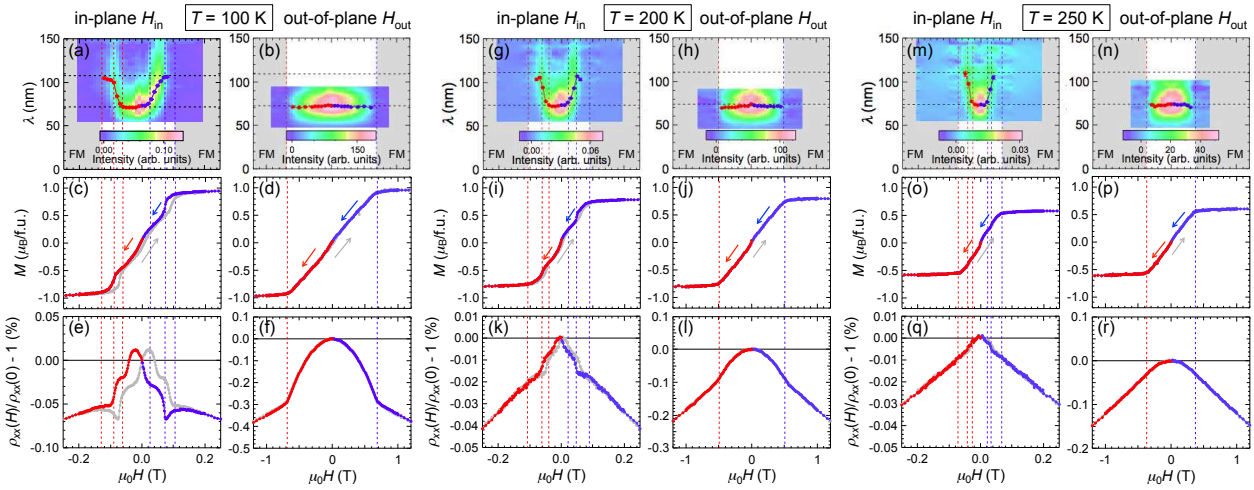

FIG. 6: Data sets for magnetic modulation period λ, magnetization M, and magnetoresistivity under in-plane and out-of-plane magnetic fields at various temperatures. Scattering patterns at $\mu_0 H_{\rm in} = 0.25$ T and at $\mu_0 H_{\rm out} = 1.0$ T at respective temperatures were used as a background subtracted from the measured patterns under the different field directions.